Solid Freeform Fabrication 2018: Proceedings of the 29th Annual International Solid Freeform Fabrication Symposium – An Additive Manufacturing Conference
Reviewed Paper

EFFECT OF IN-SITU COMPACTION AND UV-CURING ON THE PERFORMANCE OF GLASS FIBER-REINFORCED POLYMER COMPOSITE CURED LAYER BY LAYER

Shiferaw D. Beyene*, Beshah Ayalew* and Srikanth Pilla*†
*Clemson University, International Center for Automotive Research
4 Research Drive
Greenville, SC 29607
†Department of Materials Science and Engineering, Clemson University,
Clemson, SC, 29634

Abstract

In this paper, the effect of in-situ compaction and UV-induced curing on the performance of fiber-reinforced diglycidyl ether bisphenol A (DGEBA) based epoxy is studied for a layer-by-layer curing process. The optimum percentage of photo-initiator concentration and UV-intensity were obtained by conducting a different experiment for each of them. Fourier Transform Infrared (FTIR) spectroscopy method is used to determine the degree of cure. Then, short beam shear (SBS) test is conducted to measure the inter-laminar shear strength of the cured product under different compaction load. The UV intensity and Photo-initiator concentration were kept constant during the test. The result showed that thick composite parts fabricated with in-situ compaction and UV curing process have showed increased inter-laminar shear strength with increased compaction load up to a certain point. An increase in compaction beyond this point decreased the interlaminar-shear strength.

Introduction

Additive manufacturing (AM) of fiber-reinforced composites is currently conducted by stereolithography, layer-by-layer, fused deposition modeling, selective laser sintering, and extrusion [1]. Layer by layer also called laminated object manufacturing (LOM) manufacturing is a type of additive manufacturing process which uses sheet of material and adhesive to make thick part [2]. Due to its inherent capability for handling sheet materials such as fiber reinforced composite prepregs, for producing geometrically complex near net shape objects , LOM is preferred is preferred manufacturing process among others [3]. Therefore, in the last two decades there has been a growing interest in layer-by-layer method for composite manufacturing.

The interfacial characteristics of composites fabricated by LOM was investigated by [4] and reported that interlaminar shear strength is one of the main factors affecting the overall performance of the final product. C-shaped panels, made from polymer matrix composites, were directly fabricated by curved LOM [5]. A vacuum thermoforming apparatus was applied to bond commercial prepregs. In other research, model based UV-induced stepped-concurrent curing approach for manufacturing of thick acrylate based composites was proposed [6, 7] and later validated with experiment [8].

The major issue for layer by layer manufacturing process is the difficulty of bringing adjacent layers to fully consolidate and cure [5]. It is quite important to increase the interlayer strength and reduce the void content as low as possible. A handful researchers have been studying to address

this issue, [9] studied the effect of compaction and UV exposure on the inter-laminar shear strength (ILSS) and reported that improved ILSS of the final product is achieved when the optimum ILSS and UV intensity is chosen. The concept of layer-by-layer in-situ UV processing concept to make a thick glass fiber reinforced polyester composite was studied by [10]. The effect of layer thickness on the inter-laminar shear strength on achieving better ILSS is studied. The LOM system used in previous studies require post processing operation to increase the bonding between layers [11].

In this paper, we propose a new method of UV-induced layer-by-layer composite manufacturing which uses in-situ curing and compaction to increase the ILSS. First, the optimal curing time sequence that is the switching, layering and final times are determined by optimal time control. Using these optimal times, four different samples were prepared with different pressure applied during the curing. The final degree of cure was checked by observing the FTIR of the cured samples. The inter-laminar shear strength of these samples are then investigated by short beam shear test (SBS).

The rest of the paper is organized as follows: Section II discusses the UV curing process model, Section III explain how the optimal switching time control is done. Section IV discusses the experimentation. Section V discusses the results and conclusions are included in Section VI.

Cure process model

For two-layer curing, a one-dimensional heat conduction for UV-induced cationic curing process can be illustrated by the schematic of Fig.1. Where, the first mode is from initial time till UV off, the second mode is from UV off time till the second layer is added; the third mode is from layer addition (UV on) time till the UV off time on two-layer curing and final mode is from UV off time till final cure time. At the top surface, a convective boundary condition is taken (BC1) and, insulation boundary condition is considered at the bottom and sides (BC2). As depicted in the figure, there are two switching modes: switching mode one (MS1) which is from UV on to UV off and switching mode two (MS2) which is when a layer is added on the exiting layer.

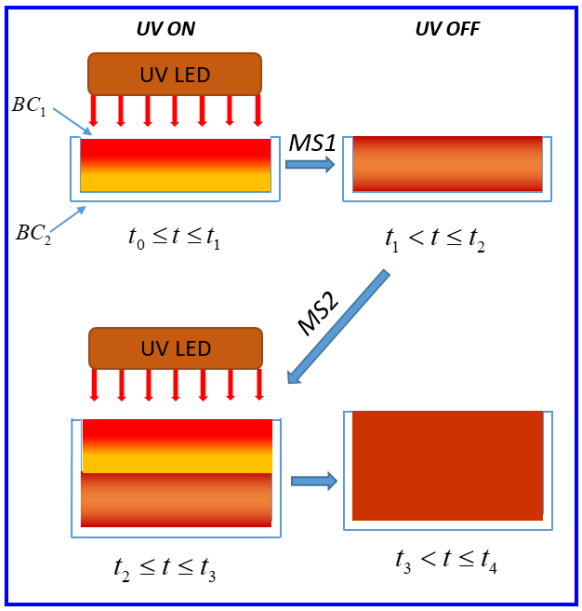

Figure 1. Schematic of cationic curing process for two layers

The process model for UV-induced cationic polymerization consists of the cure kinetic model for curing under UV and curing without UV (UV is off)). The model consists of the exothermic reaction (heat generation), conduction and convention heat transfer. The attenuation of the UV intensity along the depth is modeled by that Beer-Lambert's Law. [12, 13, 14].

The cure process model is then summarized as follows [15, 16]:

$$\rho c \frac{\partial T(t,y)}{\partial t} = k_y \frac{\partial^2 T(t,y)}{\partial y^2} + \rho_r \Delta H_r \frac{d\alpha(t,y)}{dt} \quad [1]$$

$$-k_y \frac{\partial T(t,y)}{\partial y} + \vartheta I_0 = h(T(t,y) - T_\infty) \quad [2]$$

$$\frac{\partial T(t,l)}{\partial y} = 0 \quad [3]$$

$$\frac{\partial \alpha(y,t)}{\partial t} = \begin{cases} A\exp\left(\frac{-E}{RT_{abs}}\right) I_0^p \exp(-\lambda y)\alpha^m (1-\alpha)^n, & t \in [t_0, t_s) \\ d\exp\left(\frac{-E}{RT_{abs}}\right)\left(1-e^{-k_i t_s D}\right)(1-\alpha), & t \in [t_s, t_f] \end{cases} \quad [4]$$

where ρ and c are the density and specific heat capacity of the epoxy, respectively; k_y is the thermal conductivity of the epoxy across the depth; $T(t,y)$ is the temperature at time t and depth y. ΔH is enthalpy of polymerization; $\alpha(t,y)$ is degree of cure at time t and depth y ; l is the thickness (depth) of the sample; A is pre-exponential constant; E is the activation energy ; R is universal gas constant; T_{abs} the absolute temperature in Kelvin; I_0 is the initial UV intensity; λ is UV attenuation constant; k_i is initiation rate constant; t_s and t_f are switching and final cure times.

The physical parameters used for simulation are summarized in Table 1.

TABLE1: Physical parameters for the numerical simulation

	Fraction by volume	ρ [g/cm^3]	c [J/(kg K)]	k_y [W/(cm ^{o}c)]	ΔH [J/g]
Resin	0.4	1.15	1.75	0.0025	332
Glass fiber	0.6	2.575	0.80	0.01275	-
Composite	1	2	1.02	0.0037	332

UV Transmission

The UV transmission of the epoxy resin is found by comparing the UV intensity at the top surface with the one measured at the bottom of the sample. The transmission for different photo-

initiator (PI) concentration is shown in Fig. 2. As seen in the figure the maximum absorbance is at 4% however, since the difference in the absorbance for 3% PI and 4% PI are not significantly different (<1mW/cm^2). Moreover, studies have shown that increasing the PI beyond certain level will not benefit the final degree of cure [17]. Therefore, for this study we opt for 3 % which is in agreement with literatures [18].

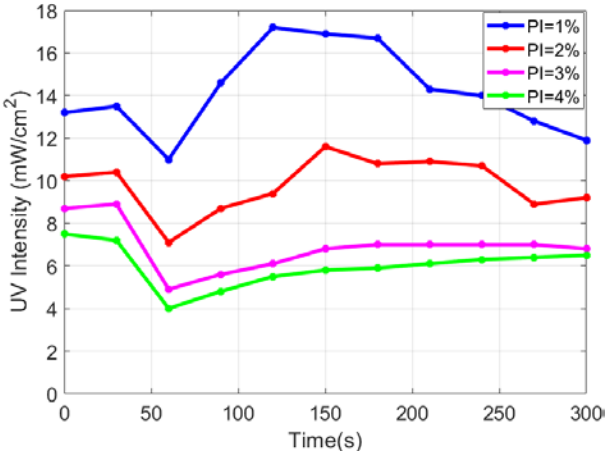

Figure 2. UV transmission for different PI concentration

Optimal switching time control

An optimal control defined as one that minimizes/maximizes some performance criteria [19]. In this paper, the objective of optimal control is to get a uniform final cure distribution. The performance measure is therefore related to what extent the actual final cure distribution deviates from the desired cure distribution. The performance measure is then given by Eq. (5)

$$J = \frac{1}{2}\int_0^l \left(\alpha(t_f) - \alpha_{des}\right)^2 dy \qquad [5]$$

where J is the performance index; $\alpha(t_f)$ is the vector containing final degree of cure at all points considered along the depth and α_{des} is the desired degree of cure along the depth at the final time t_f. l is the thickness (depth) of the sample.

Two fiber-reinforced DGEBA based prepregs with each layer 2mm thickness were considered for this study. The process input, UV intensity, is kept uniform for the first mode and turned off at the first switching time (MS1) and then it is left to cure by itself till the second switching time (MS2) this process continues for any number of layers. A one-dimensional UV-induced cationic polymerization model given in Eq. (1-4) is used to get the temperature and cure distributions along the depth. The switching times and final time are the control variables that can be optimized to get a minimum deviation of the final cure from the desired value (98%).

In our previous study, we derived the necessary conditions for optimality [16]. Similar derivations can be found in [6, 7]. The necessary conditions for optimality and the coupled PDE-ODE equations (1-4) are taken as constraints for the performance index given in Eq. (1). Steepest descent algorithm [19] was applied to find the optimal switching times and final time. The optimal switching and final times found from the optimal time control are given in Table 2.

TABLE 2. Optimal switching and final times.

Mode	1	2	3	4
Optimal switching time (s)	288	505	800	884

Experimentation

In-situ curing and compaction

Composites were fabricated by irradiating the prepreg samples using a 16.1W Clearstone UV LED which has UV emission peak wavelength of 365nm. The amount of UV reaching to the surface of the resin sample is measured by using a digital UV radiometer (Solarmeter) whose resolution is 0.1 mW/cm2. All samples were placed at the same depth from the UV LED. In our previous work [15], we verified experimentally that the optimal switching times found from simulation help to get through cure for 2mm thick resin. Hence, in this study 2mm thickness is used for a single layer. The schematic of in-situ curing and compaction is shown in Fig. 3. As depicted in the figure, the first layer is cured and then a new layer is added with a clear glass sheet on it where four equal loads are applied outside the UV exposure area. The two layers are then cured and consolidated with the in-situ pressure applied on the clear glass sheet.

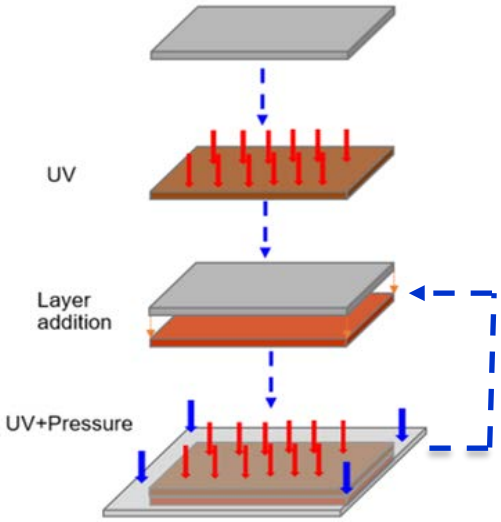

Figure 3. Schematic of in-situ compaction and curing

Final degree of cure

To make sure that the samples are completely cured, we recorded the FTIR of all cured samples and compared with the FTIR of the uncured resin. The characteristic absorptions of oxirane ring at 914.9 cm-1 is observed in the epoxy resin (before curing). This is attributed to the C-O deformation of oxirane group [20, 21]. As seen in Fig. 4 the disappearance of the band in all samples, which were manufactured with different in-situ pressure, shows that all samples are completely cured [21].

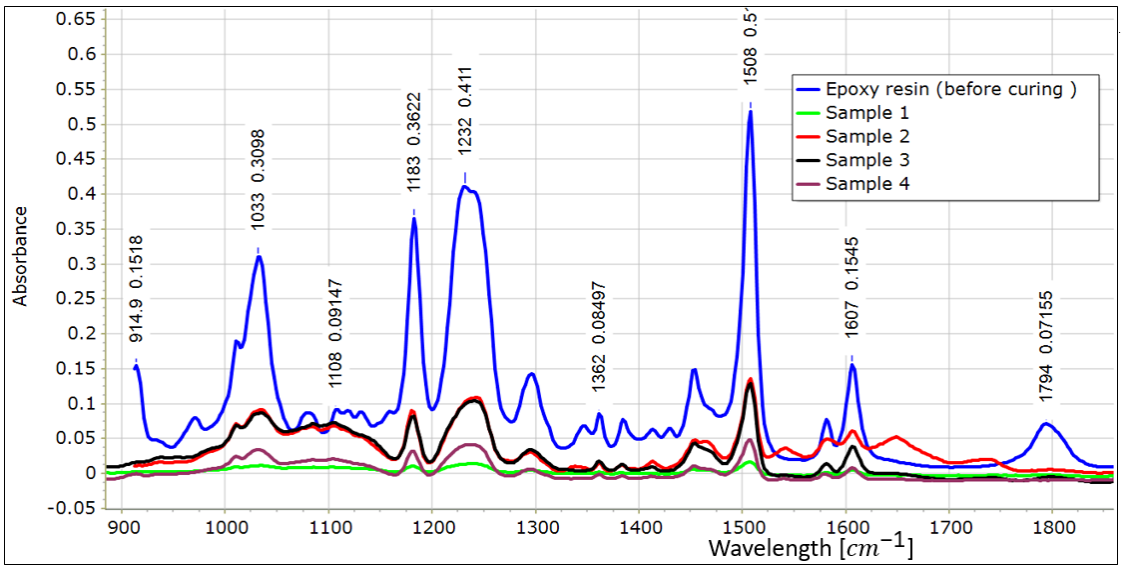

Figure 4. FTIR of all samples comared with uncured epoxy resin

Effect of pressure on ILSS

To study the effect of compaction on the interlaminar shear strength, four samples were fabricated by the in-situ curing method with varying pressure applied to the samples. Then short beam shear (SBS) test was used to measure the interlaminar shear strength for each case. The ILSS is calculate as follows [22]:

$$ILSS = 0.75 \times \frac{P_m}{b \times h} \qquad [6]$$

where ILSS is short-beam strength in MPa; P_m is the maximum load recorded during the test in Newton (N); b is the measured specimen width in mm; and h is the measured specimen thickness in mm. The maximum observed load during the SBS test and the corresponding ILSS are summarized in Table 3.

Table 3: Maximum observed load and the corresponding ILSS

Sample no.	Applied load (N)	Maximum observed load (N)	ILSS (MPa)
1	0	712.8	16.7
2	6.8	779.8	18.3
3	18.2	916.5	21.5
4	33.9	864.5	20.3

Figure 5 a) shows the maximum load observed for different loading conditions and Fig.5 b) shows the correlation between ILSS and applied load during in-situ curing. The ILSS increased by 38.75 % when the applied load increased from 0 to 18.2 N and decreases when a sample is cured under higher load. This shows that an optimum pressure is required to get better interlaminar shear strength and for our case.

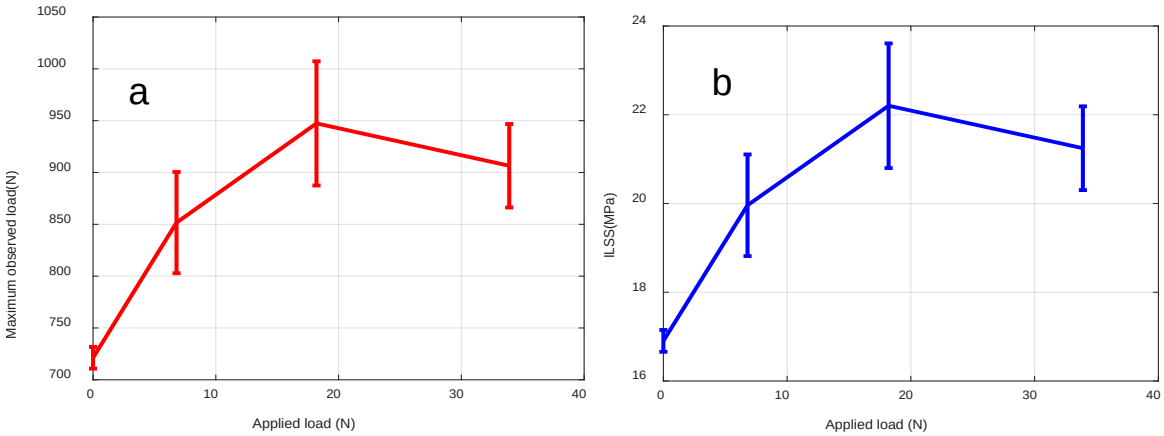

Figure 5. Maximum observed load (a) and ILLS (b) for different loading conditions.

Conclusion

In this paper, the effect of in-situ compaction and UV-induced curing on the performance of fiber-reinforced DGEBA based epoxy is studied for a layer-by-layer curing process. The optimum percentage of photo-initiator concentration is chosen for a given UV-intensity by conducting different experiment. Fourier Transform Infrared (FTIR) spectroscopy method was used to check the completeness of the final degree of cure. Then, short beam shear (SBS) test was conducted to measure the inter-laminar shear strength of the cured product under different compaction load. The curing times were found from optimal switching time control and the UV intensity and photo-initiator concentration were similar for all samples. The result showed that thick composite parts fabricated with in-situ compaction and UV curing process have showed increased inter-laminar shear strength with increased compaction load up to a certain point. An increase in compaction beyond this point decreased the interlaminar-shear strength.

Acknowledgment

This research has been supported by the National Science Foundation under grant number: CMMI-1537756

References

1. Kruth, J. P., Levy, G., Klocke, F., & Childs, T. H. C. (2007). Consolidation phenomena in laser and powder-bed based layered manufacturing. *CIRP annals*, *56*(2), 730-759.
2. Wong, K. V., & Hernandez, A. (2012). A review of additive manufacturing. ISRN Mechanical Engineering, 2012.
3. Mailunas, R. (2001). Laminated Object Manufacturing-Based Design Ceramic Matrix Composites. NORTHROP GRUMMAN CORP BETHPAGE NY.
4. Klosterman, D., Chartoff, R., Graves, G., Osborne, N., & Priore, B. (1998). Interfacial characteristics of composites fabricated by laminated object manufacturing. Composites Part A: Applied Science and Manufacturing, 29(9-10), 1165-1174.
5. Parandoush, P., & Lin, D. (2017). A review on additive manufacturing of polymer-fiber composites. Composite Structures, 182, 36-53.

6. Yebi, A., & Ayalew, B. (2015). Optimal layering time control for stepped-concurrent radiative curing process. Journal of Manufacturing Science and Engineering, 137(1), 011020.
7. Yebi, A., & Ayalew, B. (2017). Hybrid Modeling and Robust Control for Layer-by-Layer Manufacturing Processes. IEEE Transactions on Control Systems Technology, 25(2), 550-562.
8. Yebi, A., & Ayalew, B. (2016, July). Model-based optimal control of layering time for layer-by-layer UV processing of resin infused laminates. In American Control Conference (ACC), 2016 (pp. 827-832). IEEE.
9. Duan, Y., Li, J., Zhong, W., Maguire, R. G., Zhao, G., Xie, H., & Lu, B. (2012). Effects of compaction and UV exposure on performance of acrylate/glass-fiber composites cured layer by layer. Journal of Applied Polymer Science, 123(6), 3799-3805.
10. Tena, I., Arakama, J. A., Sarrionandia, M., Aurrekoetxea, J., & Torre, J. EFFECT OF THICKNESS ON THE INTERFACIAL STRENGHT OF LAYER BY LAYER IN SITU UV CURING.
11. Olivier, D., Travieso-Rodriguez, J. A., Borros, S., Reyes, G., & Jerez-Mesa, R. (2017). Influence of building orientation on the flexural strength of laminated object manufacturing specimens. Journal of mechanical science and technology, 31(1), 133-139.
12. Lee, J. (2008). Cationic polymerization of glycidyl ethers and furans: improved electron beam and UV cured epoxy networks.
13. Saldivar-Guerra, E., & Vivaldo-Lima, E. (2013). Handbook of polymer synthesis, characterization, and processing. John Wiley & Sons.
14. Endruweit, A., Johnson, M. S., & Long, A. C. (2006). Curing of composite components by ultraviolet radiation: A review. Polymer composites, 27(2), 119-128.
15. Beyene, S.D., Ayalew, B., Kousaalya, A.B. & Pilla, S. (2018). Model-based optimal switching time control of UV-induced cationic curing of diglycidyl ether bisphenol a. Society for the Advancement of Material and Process Engineering (SAMPE), Long Beach, CA.
16. Beyene, S.D., Ayalew, B., & Pilla, S. (2018). Optimal Switching Time Control of UV Induced Cationic Curing Process. In ASME 2018 Dynamic Systems and Control Conference, American Society of Mechanical Engineers. Accepted.
17. Alonso, R. C. B., de Souza-Júnior, E. J. C., Dressano, D., de Araújo, G. A. S., Rodriguez, J. M. C., Di Hipólito, V., ... & Sinhoreti, M. A. C. (2013). Effect of photoinitiator concentration on marginal and internal adaptation of experimental composite blends photocured by modulated methods. European journal of dentistry, 7(Suppl 1), S1.
18. Cho, J. D., & Hong, J. W. (2005). Photo-curing kinetics for the UV-initiated cationic polymerization of a cycloaliphatic diepoxide system photosensitized by thioxanthone. European Polymer Journal, 41(2), 367-374.
19. Kirk, D. E. (2012). Optimal control theory: an introduction. Courier Corporation.
20. González, M. G., Cabanelas, J. C., & Baselga, J. (2012). Applications of FTIR on epoxy resins-identification, monitoring the curing process, phase separation and water uptake. In Infrared Spectroscopy-Materials Science, Engineering and Technology. InTech.
21. Cherdoud-Chihani, A., Mouzali, M., & Abadie, M. J. M. (2003). Study of crosslinking acid copolymer/DGEBA systems by FTIR. Journal of applied polymer science, 87(13), 2033-2051.

22. Fan, Z., Santare, M. H., & Advani, S. G. (2008). Interlaminar shear strength of glass fiber reinforced epoxy composites enhanced with multi-walled carbon nanotubes. Composites Part A: Applied Science and Manufacturing, 39(3), 540-554